INTERFEROMETRIC TIME REVERSAL MUSIC FOR SMALL SCATTERER LOCALIZATION

R. Solimene[*], A. Dell'Aversano, and G. Leone

Dipartimento di Ingegneria dell'Informazione, Seconda Università di Napoli, I 81031 via Roma 29, Aversa, Italy

Abstract—The problem of localizing small scatterers (in terms of wavelength) by Time Reversal-MUSIC (TR-MUSIC) algorithm is addressed. In particular, we focus on uniqueness problems that might arise for certain far zone configurations when noise corrupts data. These lead to reconstructions affected by ghost targets from which it is difficult to discern actual targets. In order to remedy such a drawback, data obtained at multiple frequencies are employed. In detail, a new multi-frequency version of TR-MUSIC is introduced. It consists in mixing reconstructions obtained at different frequencies. Numerical analysis shows that this method outperforms classical TR-MUSIC as well as its multi-frequency implementation already present in literature.

1. INTRODUCTION

Radar imaging is a pervasive research field which is of interest in different applicative contexts, both military and civilian [1–6].

The common mathematical rationale is the electromagnetic scattering equations that must be solved for an object function that accounts for the scatterer features.

As is well known, this entails solving a non-linear and ill-posed inverse problem that must be attacked as an optimization one. Accordingly, inversion schemes developed along this path suffer from local minima problem and are, despite advancement in computer science, still computationally intensive to limit their usefulness in many practical cases, particularly when large (in terms of wavelength) spatial region must be quickly investigated.

Fortunately, in many cases, only *qualitative* information like scatterers' positions and sizes is of concern [7]. This allows to

adopt inversion schemes based on simplified linearized scattering equations [8, 9]. Even though they avoid drawbacks affecting non-linear inversions, reconstructions suffer from artifacts due to mutual scattering (between scatterers) that is neglected in simplified models [10].

Some other methods allow for scatterer localization by identifying their supports according to the value of a suitable indicator function [11–13]. These methods are algorithmically based on linear procedures hence are computationally effective. Moreover, they do not rely on simplified scattering models.

With reference to small (in terms of wavelength) scatterers, we focus on Time Reversal MUSIC (TR-MUSIC) that has proved to be very effective in scatterer localization as it allows to obtain resolution which is finer than diffraction limits [14]. At the beginning, TR-MUSIC has been developed for a homogeneous two-dimensional scalar scattering scene [14]. Then, extension to more complicated cases have followed. For example in [15, 16], non-homogeneous host media are considered whereas in [17] non-isotropic scatterers are addressed. Three-dimensional small scatterers are considered in [18, 19]. A comparison against background uncertainties of different time reversal and MUSIC based algorithms for small scatterers localization is instead reported in [20].

In [21], it was shown that for a far zone configuration and for data collected over an array of uniformly spaced sensors, TR-MUSIC can suffer from uniqueness problems due to the noise. Accordingly, reconstructions are affected by ghost targets in the same vain as an array radiation pattern experiences grating lobes. Analogous problems are encountered in radar range imaging due to the relationship between the frequency step and the maximum non-ambiguous range [22].

In [21], propagation through ionosphere helped in removing those ambiguities.In general this might not be the case. For such situations, Devaney suggested to exploit frequency diversity. Therefore, inspired by this suggestion, here we analyze how to exploit multiple frequencies in order to restore uniqueness and hence suppress ghost targets.

A multifrequency version of TR-MUSIC, called wide band TR-MUSIC (WBTR-MUSIC) has been already presented in [20, 23].

In this paper, we propose a different strategy. In particular, two or more reconstructions of the same scene obtained at different frequencies are "beated" in order to remove spurious targets.

We termed our method to exploit frequency diversity as Interferometric TR-MUSIC (ITR-MUSIC). This is because it resembles some interferometric inversion scheme where, however, mixing is achieved on data space rather than on reconstructions.

The paper is organized as follows. In Section 2, we recall basic theory of TR-MUSIC and discuss about uniqueness problems arising in far zone configuration [21]. In Section 3, multifrequency implementations of TR-MUSIC are described. In particular, first we report the WBTR-MUSIC [23]. Then, we introduce the new ITR-MUSIC. In Section 4, numerical examples for configurations resembling the ones reported in [21] are used to compare TR-MUSIC, WBTR-MUSCI and ITR-MUSIC. Conclusions end the paper.

2. TR-MUSIC

The general scenario consists of one or more isolated point targets located at position $\underline{r}_m$, $m = 1, 2, \ldots, M$ within a background medium characterized by an outgoing wave scalar Green function $G\left(\underline{r}, \underline{r}', f\right)$, f denoting the temporal frequency.

Targets are assumed to be interrogated by an array of antennas having N transmitting and receiving elements. As in [13], we assume they are co-located at the observation points $\underline{\alpha}_k$, $k = 1, 2, \ldots, N$. Moreover, $N > M$.

For each transmitting antenna, the scattered field is collected over all the array antennas and arranged to form the so called $N \times N$ multistatic data matrix (MDM) $\mathbf{K}$. Accordingly, its $\{j, k\}$ element $K_{j,k}$ is the scattered field $E_S\left(\cdot\right)$ evaluated at $\underline{\alpha}_j$ once antenna in $\underline{\alpha}_k$ probes the scene.

The multistatic data matrix operator

$$\mathbf{K}: \quad C^N \to C^N \tag{1}$$

is an endomorphism over the complex linear space C^N. Accordingly, $C^N = R(\mathbf{K}) \oplus N(\mathbf{K})$ can be decomposed as the direct sum of two orthogonal manifolds given by the range $R(\mathbf{K})$, denoted as *signal subspace*, and its orthogonal complement $N(\mathbf{K})$, called the *noise sunspace* of $\mathbf{K}$.

Under ideal conditions (no noise and numerical uncertainties) singular values $\sigma_n = 0$ if $n > M$, that is the rank of $\mathbf{K}$, coincides with the number of scatterers (unless some pathological configurations [24] are met). Therefore, it results that,

$$
\begin{aligned}
R(\mathbf{K}) &= span\{\mathbf{u}_1, \mathbf{u}_1 \cdots, \mathbf{u}_M\} \\
N(\mathbf{K}) &= span\{\mathbf{u}_{M+1}, \mathbf{u}_{M+2} \cdots, \mathbf{u}_N\}
\end{aligned}
\tag{2}
$$

where $\{\mathbf{u}_n\}_{n=1}^N$ and M are the left singular vectors and the rank of $\mathbf{K}$, respectively.

The multistatic data matrix can be factorized as follows

$$\mathbf{K} = \mathbf{G}\mathbf{H}^{-1}\mathbf{G}^T \tag{3}$$

where ^{T} represents the transpose operator, $\mathbf{G}$ is the $N \times M$ propagator matrix from scatterers to the observation points whose n-th column is $\mathbf{g}_n = [G(\underline{\alpha}_1, \underline{r}_n), G(\underline{\alpha}_2, \underline{r}_n), \cdots, G(\underline{\alpha}_N, \underline{r}_n)]^T$ and $\mathbf{H}^{-1}$ is the matrix that takes into account interactions between scatterers, according to Foldy-Lax model [25].

From Eq. (3), it is clear that $span\{\mathbf{g}_1, \mathbf{g}_1 \cdots, \mathbf{g}_M\} \subseteq R(\mathbf{K})$. Therefore, scatterers' positions can be identified as the locus where the pseudospectrum

$$P(\underline{r}) = \frac{1}{\displaystyle\sum_{\sigma_j=0} |\mathbf{u}_j^H \mathbf{g}(\underline{r})|^2} \tag{4}$$

peaks. Here, ^{H} means the Hermitian and $\underline{r}$ ranges within the investigation domain where the scatterers are assumed to reside.

2.1. Ghost Targets

When noise corrupts data, TR-MUSIC performance can deteriorate [26].

First, rank of $\mathbf{K}$ tends to increase making it difficult to discern between the noise and the signal subspaces. Here, however, we assume the signal to noise ratio is sufficiently high to let one able to identify the sharp transition occurring between the signal and noise singular values. Alternatively, more sophisticated method can be applied to estimate it [27].

Noise also affects noise subspace structure. This can give rise to phantom scatterers appearing in the reconstructions.

To show this, we follow Devaney arguments [21].

Consider a homogeneous background medium and assume that both the observation and the investigation domains consist of parallel segments, and that sensors are taken uniformly at spatial step δ. This means that $\underline{\alpha}_k \equiv (x_k, 0, z)$, where $x_k = -X_O + (k-1)\delta$, X_O being the semi-extent of the observation segment. Targets' position are instead $\underline{r}_n \equiv (x_n, 0, 0)$ with $-X_I \leq x_n \leq X_I$, X_I being the semi-extent of the investigation domain.

When noise corrupts data, differences between steering vectors corresponding to scatterers located at x_n and $x_n + mL$, with

$$L = \frac{\lambda z}{\delta} \tag{5}$$

and λ being the wavelength, tend to be smoothed. Therefore, pseudospectrum in Eq. (4) shows multiple peaks and it is no more possible to uniquely determine the positions of targets using a single

frequency [21]. This can be roughly explained by recalling far zone approximation of the Green's function

$$G\left(\underline{\alpha}_k, \underline{r}_n\right) \cong 1/z \exp\{-ik_0[z + (x_k^2 + x_n^2)/2z]\} \exp(ik_0 x_k x_n/z) \quad (6)$$

In particular, the occurrence of replicas is due to the second exponential term appearing in the right-hand side of (6), entailing periodicity.

An illustrative example of this situation is shown in Fig. 1. This figure reports the reconstruction of a single target located at $(-4, 0, 0)$ m within an investigation domain with $X_I = 50$ m, for noiseless (top panel) and noisy data (bottom panel). To achieve that, a fixed frequency of $f = 2$ GHz is employed whereas the measurement array consists of $N = 5$ antennas located at $x_k = [-4, -2, 0, +2, +4]$ m (i.e., $X_O = 4$ m) for $z = h = 190$ m. Data have been corrupted by an additive white Gaussian noise $\mathbf{N}$ with $SNR = 40$ dB. The signal to noise ratio is defined as $SNR = 20 \log\left(\|\mathbf{K}\|_F / \|\mathbf{N}\|_F\right)$, where $\|\cdot\|_F$ being the Frobenius norm. Note that, due to the high dynamic exhibited by the peseudosprectum in Eq. (4) results are displayed under logarithmic normalized convention, that is

$$P_{\text{dB}}\left(\underline{r}\right) = 20 \log \frac{P\left(\underline{r}\right)}{\max\{P\left(\underline{r}\right)\}} \quad (7)$$

As can be seen, reconstruction is perfect for noiseless data. However, even though the SNR is relatively high for noisy data replicas appear at a period just equal to $L = 14.27$ m, according to Eq. (5).
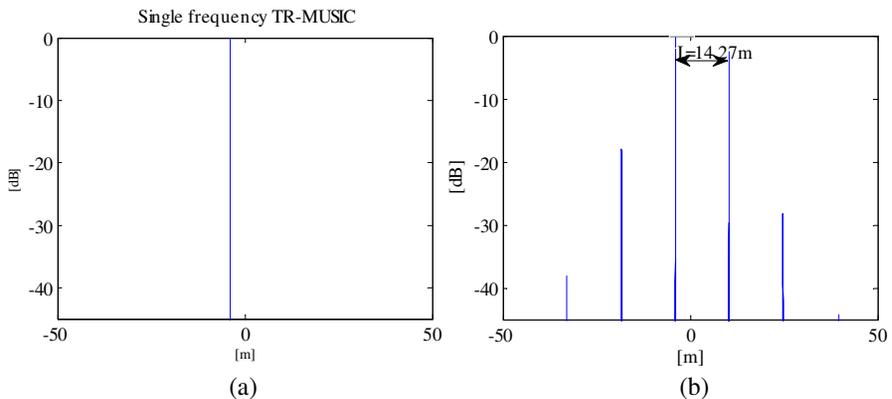
Figure 1. Single target pseudospectrum P_{dB}. (a) Reconstruction without noise. (b) Reconstruction with noise.

3. MULTIFREQUENCY TR-MUSIC

To overcome the above mentioned non-uniqueness problem, in [21], it is taken advantages from propagation through a ionosphere layer that greatly diminished grating lobe effects. This is because the strict periodic structure of the far field Green function implied by (6) is destroyed.

When this circumstance does not occur, TR-MUSIC algorithm has to be modified in order to properly work also in these cases.

To this end, frequency diversity can be exploited. Indeed, from previous section it is seen that target replicas appear at positions which depend on the working frequency. Therefore, if multiple frequency data are suitably combined their presence can be in some way *averaged* and hence mitigated.

In this regard, it is worth mentioning that a multi-frequency version of TR-MUSIC, the WBTR-MUSIC, has been already presented in literature [20, 23]. In those papers, pseudospectra, as in (4), obtained at different working frequencies are combined so that the overall scatterer position estimator is given by

$$PWB\left(\underline{r}\right) = \frac{1}{\displaystyle\int_{\Omega} \sum_{\sigma_j \leq \varepsilon} |\mathbf{u}_j^H\left(f\right)\mathbf{g}\left(\underline{r}, f\right)|^2 df} \tag{8}$$

where Ω is the employed frequency bandwidth.

Such a MUSIC version resolves some problems affecting time domain time reversal scheme without the need of further processing to compensate the arbitrary and frequency dependent phases which characterizes MDM eigenvectors [28]. Moreover, because it combines reconstructions obtained at different frequencies it is shown that this method is statistically stable [20].

Note that, as data are corrupted by noise, a suitable decision threshold ε is employed to select the noise subspace. More in detail, this is chosen by a visual inspection of the singular value behavior in correspondence of their sharper transition. Alternatively, a different criterion can be followed [27].

In this paper, we propose a different way to exploit multi-frequency data in an *interferometric* fashion.

More in detail, the multi-frequency pseudospectrum is obtained by a pixel by pixel multiplication between reconstructions obtained at different frequencies. This way to combine frequency is expected to better exploit the fact that spurious peak positions change with frequency, whereas actual target peaks do not. Accordingly, we address this method as interferometric TR-MUSIC (ITR-MUSIC) and the

corresponding pesudospectrum is given as

$$PI\left(\underline{r}\right) = \prod_{q=1}^{Q} \frac{1}{\sum_{\sigma_j \leq \varepsilon} |\mathbf{u}_j^H\left(f_q\right)\mathbf{g}\left(\underline{r}, f_q\right)|^2} \tag{9}$$

where Q is the number of chosen frequencies.

4. NUMERICAL RESULTS AND COMPARISON

In this section, the two multifrequency TR-MUSIC methods are compared according to same scenario as in Section 2 (see Fig. 1). In particular, scatterers are all assumed to have equal frequency independent scattering coefficients.

Finally, all the figures display pseudospectra under a logarithmic scale, that is

$$PWB_{\mathrm{dB}}\left(\underline{r}\right) = 20\log\frac{PWB\left(\underline{r}\right)}{\max\{PWB\left(\underline{r}\right)\}} \tag{10}$$

and

$$PI_{\mathrm{dB}}\left(\underline{r}\right) = 20\log\frac{PI\left(\underline{r}\right)}{\max\{PI\left(\underline{r}\right)\}} \tag{11}$$
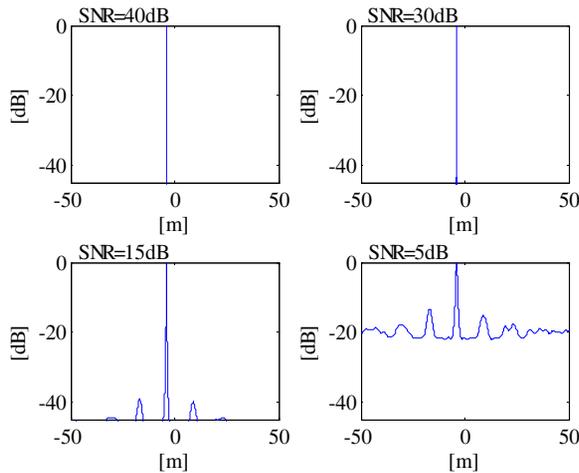
Figure 2. Single target pseudospectra PW_{dB} for different levels of SNR.
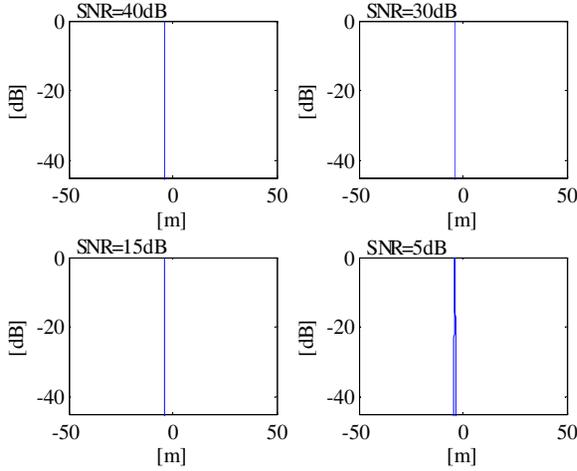
Figure 3. Single target pseudospectra PI_{dB} for different levels of SNR.

4.1. Role of Noise

As spurious artifacts are due to the noise it makes it sense first to study how WBTR-MUSIC and ITR-MUSIC perform under different values of SNR (defined as in previous section). To this end, a single target located at $(-4, 0, 0)$ is considered and five frequencies taken uniformly within the bandwidth $\Omega = [2, 2.5]\,\mathrm{GHz}$ are used. Logarithmic pseudospectra as SNR varies are reported in Fig. 2 and Fig. 3, respectively, for the WBTR-MUSIC and the ITR-MUSIC method.

As can be seen, both methods succeed in removing spurious artifacts for high values of SNR and hence outperform TR-MUSIC. However, when SNR decreases ITR-MUSIC performs better than WBTR-MUSIC which remains still affected by few ghost peaks and above all suffers from a higher clutter pedestal.

4.2. Two Target Case

In the case of two targets the scene is populated by replicas due to both of them. Moreover, noise in general will also couse loss of resolution [26].

First, it is considered the case of well-resolved scatterers. In particular, the two targets are located at $x_1 = -16\,\mathrm{m}$ and $x_2 = 21\,\mathrm{m}$, that is, well beyond diffraction limit $\lambda h/X_O$ that at the highest adopted frequency of 2.5 GHz is equal to 5.7 m. Also in this case, from Fig. 4
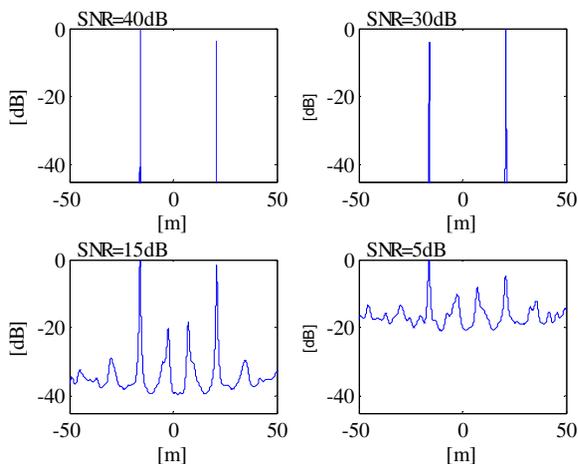
Figure 4. Two target pseudospectra PWB_{dB} for different levels of SNR. Targets are separated by a distance of 37 m.

Figure 5. Two target pseudospectra PI_{dB} for different levels of SNR. Targets are separated by a distance of 37 m.

and Fig. 5, it can be appreciated how for low SNR ITR-MUSIC performs better than WBTR-MUSIC. In particular, for SNR = 5 dB, WBTR-MUSIC returns an high cluttered reconstruction with peaks comparable to those of actual targets. For this SNR, ITR-MUSIC also is cluttered but spurious peaks are still many dB below target peaks.

In the second example (Figs. 6 and 7), targets get closer, below

diffraction limit. They are located at $x_1 = 4\,\mathrm{m}$ and $x_2 = 6\,\mathrm{m}$. Also in this case it can be concluded that ITR-MUSIC is more stable against noise.
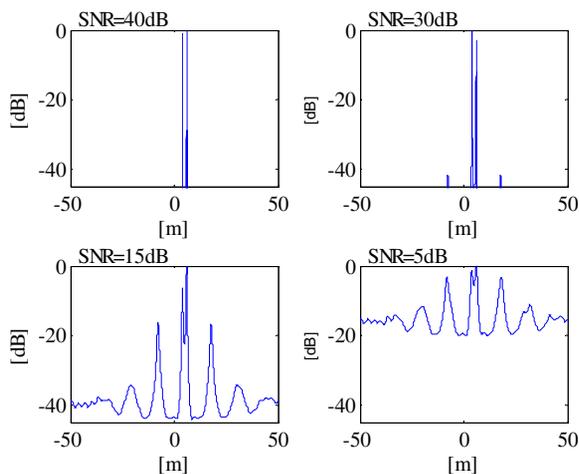
Figure 6. Two target pseudospectra PWB_{dB} for different levels of SNR. Targets are separated by a distance of $2\,\mathrm{m}$.
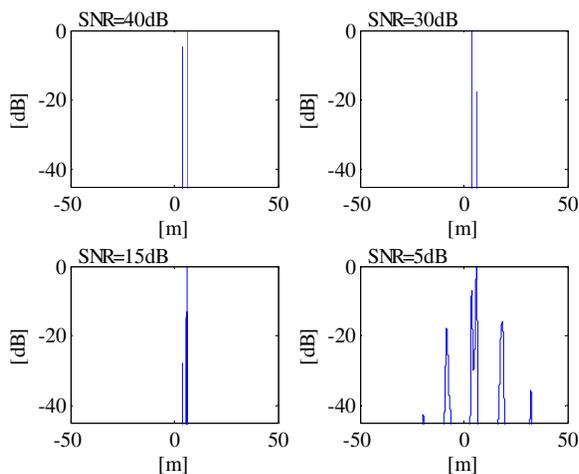
Figure 7. Two target pseudospectra PI_{dB} for different levesl of SNR. Targets are separated by a distance of $2\,\mathrm{m}$.

4.3. Role of Frequency Allocation

According to Eq. (5), the number of replicas increases as frequency grows (or equivalently by enlarging the measurement aperture keeping fixed the number of antennas). Therefore, it is worth investigating how WBTR-MUSIC and ITR-MUSIC behave in such a case.

To this end, the same case as in Figs. 6 and 7 is addressed but the five frequencies are taken within the band $\Omega = [3, 3.5]$ GHz. The corresponding reconstructions are reported in Figs. 8 and 9. Actually, for WBTR-MUSIC the lower SNR the higher number of replicas. However, ITR-MUSIC remains rather stable with a slightly improvement in resolution due to the adopted higher frequencies. In any case, the latter shows better performance.

4.4. Role of Number of Frequencies

Previous examples shown that ITR-MUSIC still remains affected by spurious artifacts in the case of two targets when SNR is very low (see Figs. 7 and 9). Instead, this circumstance does not occur for the case of single target (see Fig. 3). This can be roughly explained by observing that in the case of two targets there are two different set of replicas. Therefore, it can occur that some replicas overlap at some points making high the pseudospectrum in those positions. This, of course, depends on actual scatterers' positions and on the adopted frequencies.
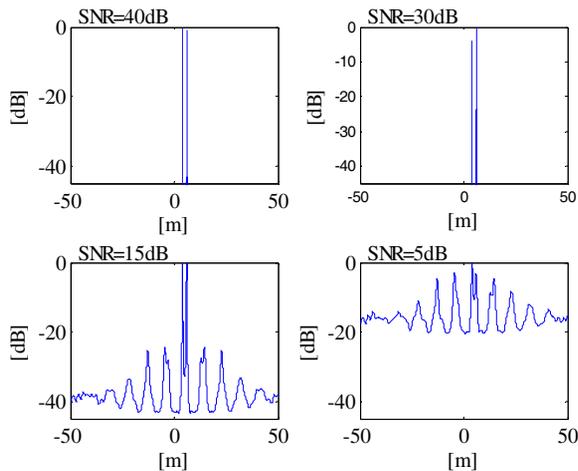
Figure 8. Two target pseudospectra PWB_{dB} for different level of SNR. Targets are separated by a distance of 2 m and $\Omega = [3, 3.5]$ GHz.
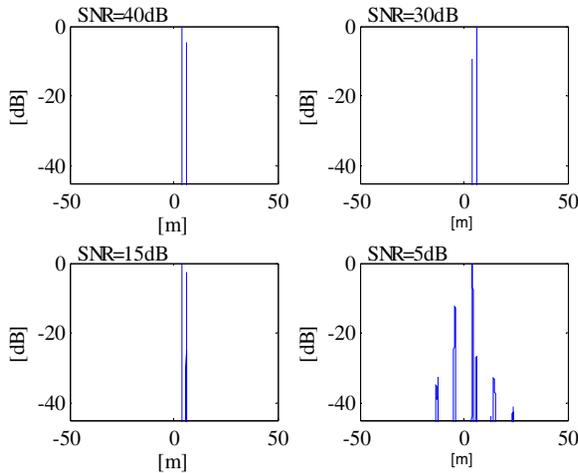
Figure 9. Two target pseudospectra PI_{dB} for different level of SNR. Targets are separated by a distance of 2 m and $\Omega = [3, 3.5]$ GHz.

In order to mitigate such a drawback the number of frequencies can be increased. Indeed, by doing so, it is expected that while pseudospectra at different frequencies will certainly overlap in correspondence to actual targets' positions throughout the entire bandwidth, spurious replicas will overlap only for few frequencies. Hence, it is expected that the dynamic range between actual scatterer reconstructions and spurious peaks increases. Accordingly, this will make artifacts only barely visible or at best they can completely disappear.

In order to show the effectiveness of this strategy, the case of not well resolved scatterers addressed in Figs. 7 and 9 is considered. In particular, only results concerning the more critical situation for SNR= 5 dB are shown. PWB_{dB} and PI_{dB} are displayed in Figs. 10 and 11, respectively. There, different frequency allocations are considered and the number of adopted frequencies is increased up to 10. As can be seen, above conjecture is very well verified. Indeed, ITR-MUSIC images appear more clear as compared to the corresponding reported in Figs. 7 and 9. Moreover, the proposed ITR-MUSIC returns clearer reconstructions and allows to obtain values of signal-to-clutter ratio higher than WBTR-MUSIC.
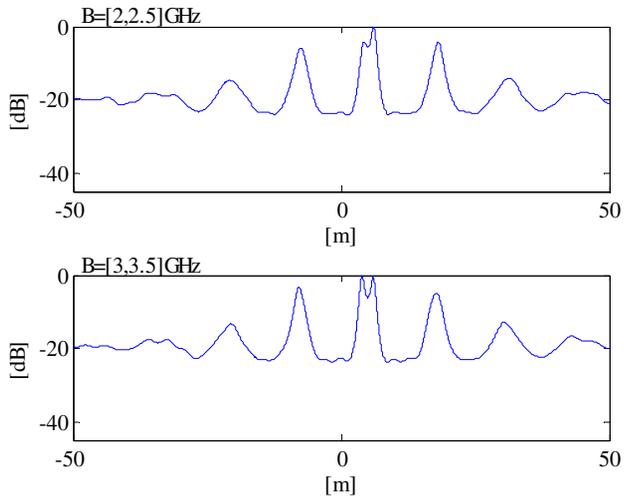
Figure 10. Two target pseudospectra PWB_{dB} for SNR $= 5\,\mathrm{dB}$ and 10 adopted frequencies.
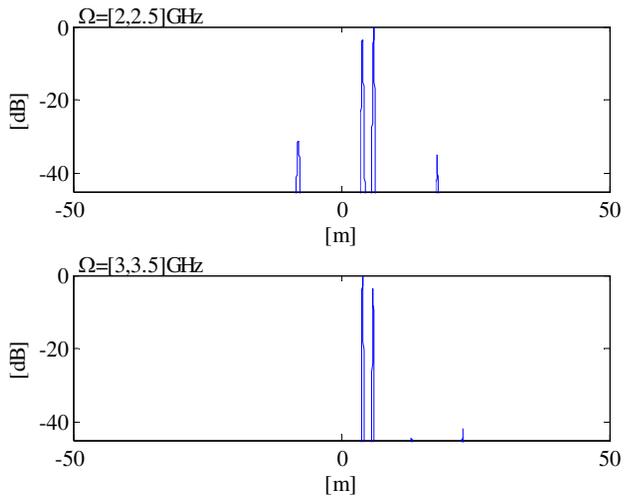
Figure 11. Two target pseudospectra PI_{dB} for SNR $= 5\,\mathrm{dB}$ and 10 adopted frequencies.

5. CONCLUSION

As outlined in [21], single-frequency TR-MUSIC can suffer from uniqueness problems when noise corrupts data for some far zone configurations. Here, we propose a new TR-MUSIC detection algorithm based on interferomentric arguments. This allowed to remove unwanted targets replicas by outperforming TR-MUSIC multi-frequency implementation already present in literature.

Of course, material conveyed in this paper has to be mainly meant as a proof of concept as a highly idealized scattering scenario has been considered.

It is our future commitment to consider more realistic situations and proceed to the mandatory experimental validation.

REFERENCES

1. Semnani, A. and M. Kamyab, "Truncated cosine fourier series expansion method for solving 2-d inverse scattering problems," *Progress In Electromagnetics Research*, Vol. 81, 73–97, 2008.
2. Solimene, R., A. Brancaccio, R. Pierri, and F. Soldovieri, "TWI experimental results by a linear inverse scattering approach," *Progress In Electromagnetics Research*, Vol. 91, 259–272, 2009.
3. Park, J. I. and K. T. Kim, "A comparative study on isar imaging algorithms for radar target identification," *Progress In Electromagnetics Research*, Vol. 108, 155–175, 2010.
4. Zhang, W., A. Hoorfar, and L. Li, "Through-the-wall target localization with time reversal music method," *Progress In Electromagnetics Research*, Vol. 106, 75–89, 2010.
5. Solimene, R., A. Brancaccio, R. Di Napoli, and R. Pierr, "3D sliced tomographic inverse scattering experimental results," *Progress In Electromagnetics Research*, Vol. 105, 1–13, 2010.
6. Zhu, X., Z. Zhao, W. Yang, Y. Zhang, Z. Nie, and Q. H. Liu, "Iterative time-reversal mirror method for imaging the buried object beneath rough ground interface," *Progress In Electromagnetics Research*, Vol. 117, 19–33, 2011.
7. Xiao, S., J. Chen, X. Liu, and B. Z. Wang, "Spatial focusing characteristics of time reversal UWB pulse transmission with different antenna array," *Progress In Electromagnetics Research B*, Vol. 2, 223–232, 2008.
8. Lopez-Sanchez, J. M. and J. Fortuny-Guash, "3-D radar imaging using range migration techniques," *IEEE Trans. Antennas Propag.*, Vol. 48, No. 5, 728–737, May 2000.

9. Solimene, R., A. Buonanno, F. Soldovieri, and R. Pierri, "Physical optics imaging of 3D PEC objects: Vector and multipolarized approaches," *IEEE Trans, Geosc. Rem. Sen.*, Vol. 48, 1799–1808, 2010.

10. Solimene, R., A. Brancaccio, J. Romano, and R. Pierri, "Localizing thin metallic cylinders by a 2.5-D linear distributional approach: Experimental results," *IEEE Trans. Antennas Propag.*, Vol. 56, 2630–2637, 2008.

11. Potthast, R., "Asurvey on sampling and probe methods for inverse problems," *Inverse Problems*, Vol. 22, R1–R47, 2006.

12. Gruber, F. K., E. A. Marengo, and A. J. Devaney, "Time-reversal imaging with multiple signal classification considering multiple scattering between the targets," *J. Acoust. Soc. Am.*, Vol. 115, 3042–3047, 2004.

13. Park, W. K., "Non-iterative imaging if thin electromagnetic inclusions from multi-frequency response matrix," *Progress In Electromagnetics Research*, Vol. 106, 225–241, 2010.

14. Lehman, S. K. and A. J. Devaney, "Transmission mode time-reversal super-resolution imaging," *J. Acoust. Soc. Am.*, Vol. 113, 2742–2753, 2003.

15. Ammari, H., E. Iakovleva, and D. Lesselier, "A music algorithm for locating small inclusions buried in a half-space from the scattering amplitude at a fixed frequency," *Multiscale Modeling and Simulation*, Vol. 3, 597–628, 2005.

16. Agarwal, K., L. Pan, Y. K. Leong, M. Han, O. Y. Chan, X. Chen, and S. P. Yeo, "Practical application of multiple signal classification," *Int. J. RF Microw. Comptuter-Aided Eng.*, Vol. 22, 359–369, 2012.

17. Chen, X. and K. Agarwal, "MUSIC algorithm for two-dimensional inverse problems with special characteristics of cylinders," *IEEE Trans. Antennas Propag.*, Vol. 56, No. 6, 1808–1812, 2008.

18. Ammari, H., E. Iakovleva, D. Lesselier, and G. Perrusson, "Music-type electromagnetic imaging of a collection of small three-dimensional inclusions," *SIAM J. Scient. Comp.*, Vol. 29, 674–709, 2007.

19. Chen, X. and Y. Zhong, "MUSIC electromagnetic imaging with enhanced resolution for small inclusions," *Inverse Problems*, Vol. 25, 2009.

20. Yavuz, M. E. and F. L. Teixeira, "On the sensitivity of time-reversal imaging techniques to model perturbations," *IEEE Trans. Antennas Propag.*, Vol. 56, No. 3, 834–843, 2008.

21. Devaney, A. J., "Time reversal imaging of obscured targets from multistatic data," *IEEE Trans. Antennas Propag.*, Vol. 53, No. 5, 1600–1610, 2005.

22. Gu, X. and Y. H. Zhang, "Resolution threshold analysis of MUSIC algorithm in radar range imaging," *Progress In Electromagnetics Research B*, Vol. 31, 297–321, 2011.

23. Lev-Ary, H. and D. J. Devaney, "The time-reversal technique re-interpreted: Subspace-based signal processing for multi-static target location," *Proc. of IEEE Sensor Array and Multichannel Signal Processing Workshop*, 2000.

24. Marengo, E. A. and F. K. Gruber, "Subspace-based localization and inverse scattering of multiply scattering point targets," *EURASIP Journal on Advances in Signal Processing*, Vol. 2007, 16 pages, 2007.

25. Foldy, L. L., "The multiple scattering of waves," *Phys. Rev.*, Vol. 67, 107–119, 1945.

26. Davy, M., J. G. Minonzio, J. De Rosny, C. Prada, and M. Fink, "Influence of noise on subwavelength imaging of two close scatterers using time reversal method: Theory and experiments," *Progress In Electromagnetics Research*, Vol. 98, 333–358, 2009.

27. Pourahmadi, M., M. Nakhkash, and A. A. Tadion, "Application of MDL criterion for microwave imaging by MUSIC algorithm," *Progress In Electromagnetics Research B*, Vol. 40, 261–278, 2012.

28. Yavuz, M. E. and F. L. Teixeira, "Space-frequency ultrawideband time-reversal imaging," *IEEE Trans. Geosc. Rem. Sen.*, Vol. 46, 1115–1124, 2008.